Bioactive-glass ceramic with two crystalline phases (BioS-2P) for bone tissue engineering

2017 Biomed. Mater. 12 045018

(http://iopscience.iop.org/1748-605X/12/4/045018)

Biomedical Materials

RECEIVED
13 March 2017

REVISED
17 May 2017

ACCEPTED FOR PUBLICATION
2 June 2017

PUBLISHED
9 August 2017

PAPER

Bioactive-glass ceramic with two crystalline phases (BioS-2P) for bone tissue engineering

Emanuela Prado Ferraz[1], **Gileade Pereira Freitas**[1], **Murilo Camuri Crovace**[2], **Oscar Peitl**[2], **Edgar Dutra Zanotto**[2], **Paulo Tambasco de Oliveira**[1], **Marcio Mateus Beloti**[1] **and Adalberto Luiz Rosa**[1]

[1] Cell Culture Laboratory, School of Dentistry of Ribeirão Preto, University of São Paulo, Ribeirão Preto, SP, Brazil
[2] Vitreous Materials Laboratory, Department of Materials Engineering, Federal University of São Carlos, São Carlos, SP, Brazil

E-mail: adalrosa@forp.usp.br

Keywords: bioactive glass-ceramic, Biosilicate®, bone, mesenchymal stem cell, osteoblast, scaffold

Abstract

We aimed to evaluate the *in vitro* osteogenic and osteoinductive potentials of BioS-2P and its ability to promote *in vivo* bone repair. To investigate osteogenic potential, UMR-106 osteoblastic cells were cultured on BioS-2P and Bioglass 45S5 discs in osteogenic medium. The osteoinductive potential was evaluated using mesenchymal stem cells (MSCs) cultured on BioS-2P, Bioglass 45S5 and polystyrene in non-osteogenic medium. Rat bone calvarial defects were implanted with BioS-2P scaffolds alone or seeded with MSCs. UMR-106 proliferation was similar for both materials, while alkaline phosphatase (ALP) activity and mineralization were higher for BioS-2P. Bone sialoprotein (BSP), RUNX2 and osteopontin (OPN) gene expression and BSP, OPN, ALP and RUNX2 protein expression were higher on BioS-2P. For MSCs, ALP activity was higher on Bioglass 45S5 than on BioS-2P and was lower on polystyrene. All genes were highly expressed on bioactive glasses compared to polystyrene. BioS-2P scaffolds promoted *in vivo* bone formation without differences in the morphometric parameters at 4, 8 and 12 weeks. After 8 weeks, the combination of BioS-2P with MSCs did not increase the quantity of new bone compared to the BioS-2P alone. To stimulate osteoblast activity, drive MSC differentiation and promote bone formation, BioS-2P is a good choice as a scaffold for bone tissue engineering.

1. Introduction

Over the past decade, tissue engineering based on combinations of cells and biomaterials has been investigated as a feasible strategy for bone regeneration. One of the frontiers for this cell-based therapy is the development of scaffolds that act as templates to guide bone growth. The ideal scaffold should have favourable biological and mechanical properties with a suitable surface to stimulate cell adhesion, proliferation and differentiation, biodegradability and adequate mechanical strength [1–4].

Since 1969, when Hench discovered the melt-derived bioactive glass, which is called Bioglass 45S5, many investigations have been performed aimed at its different biological applications [5, 6]. A major step development in this field was the demonstration that bioactive glasses can bond to living bone [7]. More recently, the term 'osteostimulation' was coined to refer to the mechanisms triggered by bioactive glasses in the body to repair bone [5, 8]. Despite the outstanding biological properties of Bioglass 45S5, which is available in several forms including porous blocks, the generation of scaffolds with improved mechanical strength without affecting biocompatibility has been a key challenge in the scientific community [9–13].

In this scenario, the development of new glass formulations to overcome this mechanical limitation would be very welcome. A glass-ceramic with the composition $23.75Na_2O$–$23.75CaO$–$48.5SiO_2$–$4P_2O_5$ (wt%) named Biosilicate® was created to combine bioactivity properties with mechanical strength [14]. Under controlled heat treatment, Biosilicate® can be produced with one (BioS-1P) or two (BioS-2P) crystalline phases that have an associated increase in the elastic modulus and fracture strength [15, 16]. BioS-1P increases *in vitro* extracellular matrix mineralization in an osteogenic cell culture system and preserves the dental alveolar ridge height, which allowed for titanium implant osseointegration in a pre-clinical animal model [17, 18]. The BioS-2P can be produced as

scaffolds and exhibits a similar response to BioS-1P and Bioglass 45S5 in terms of contact with bone [19].

Several biological and mechanical features make Biosilicate® an appealing candidate to fabricate scaffolds for bone regeneration. However, the effects of this secondary crystalline phase are underexplored and need to be investigated. Thus, the aim of this study was to evaluate both the *in vitro* osteogenic and osteoinductive potentials of BioS-2P and their effects on *in vivo* bone repair. Furthermore, we evaluated if BioS-2P scaffold combined with mesenchymal stem cells (MSCs) could improve bone formation.

2. Materials and methods

2.1. Sample preparation and characterization

High-purity silica (Zetasil 3, Santa Rosa Mineração, Pequeri, MG, Brazil) and reagent grade calcium carbonate (JT Baker, Center Valley, PA, USA), sodium carbonate (JT Baker), and monosodium phosphate (JT Baker) were used to produce Biosilicate® parent glass and Bioglass 45S5. The chemicals were blended overnight and then they were melted in a platinum crucible at 1450 °C for 4 h, splat-cooled and re-melted three times (every 1 h). Finally, the melts were cast into a cylindrical stainless steel mould 50 mm in height by 12 mm in diameter. Biosilicate® parent glass was fully crystallized using a double stage heat-treatment first for crystal nucleation (565 °C/100 h) and then for crystal growth (665 °C/1 h). To obtain Biosilicate® containing two crystalline phases (BioS-2P), an additional heat-treatment was performed at 800 °C/1 h. The cylinders of BioS-2P glass-ceramic and Bioglass 45S5 were cut into 3 mm thick discs. The discs were ground using silicon carbide paper to a grit of 400 (~35 μm) and cleaned with isopropyl alcohol (99.8%) in an ultrasonic cleaner for 1 min. The scaffolds were obtained from BioS-2P as previously described [20]. Briefly, a suspension containing BioS-2P powder mixed with carbon black was dried, pressed and sintered (975 °C/5 h) to produce porous scaffolds with 5 mm in diameter and 2 mm in height. Prior to cell culture experiments and surgical procedures, all samples were submitted to sterilization using dry heat at 180 °C for 2 h.

2.1.1. X-ray diffraction (XRD) and optical microscopy

The ground solid discs (grit 400) of BioS-2P were analysed via XRD (Ultima IV, Rigaku, Japan). A step scan mode (0.01° s^{-1}), i.e., a count time of 4 s, from 10° to 90° was used. The crystalline phases present in BioS-2P were identified using Crystallographica Search-Match software (version 2.1.1.1, Oxford Cryo Systems, Murray Hill, NJ, USA). After surface-polishing, BioS-2P discs were analysed using an optical microscope (Eclipse LV100NPOL, Nikon, Japan) attached to a digital camera (DSFi2, Nikon). On the surface, images were captured using reflected light. From 1.5 to 8.5 μm below the surface, images were automatically captured every 0.1 μm using polarized light. The images were merged, and a focused 3D image was created using the imaging software NIS Elements, version 4.20 (Nikon).

2.1.2. Microtomography and morphometric analysis

BioS-2P scaffolds were evaluated by micro-CT using the SkyScan 1172 system (Bruker, Sky-Scan, Belgium). The images were generated at 60 kV and 200 mA using isotropic voxel 5.88 μm and the reconstructions were made using NRecon software (1.6.10.4 version, Bruker) with smoothing set at 1, ring artefact correction set at 5 and beam hardening correction set at 20%. Three samples were scanned to evaluate the percentage of total porosity and pore size distribution.

2.2. Osteogenic potential of BioS-2P

2.2.1. Culture of UMR-106 osteoblastic cell line

The rat osteoblastic cell line UMR-106 (American Type Culture Collection, Manassas, VA, USA) was cultivated in growth medium (non-osteogenic conditions) constituted by alpha-minimum essential medium (α-MEM, Gibco-Life Technologies, Grand Island, NY, USA) supplemented with 10% foetal bovine serum (Gibco-Life Technologies), 50 μg ml^{-1} penicillin/streptomycin (Gibco-Life Technologies) and 0.3 μg ml^{-1} fungizone (Gibco-Life Technologies). After subconfluence, cells from first passage were cultured in 24-well culture plates on BioS-2P and Bioglass 45S5 discs at a cell density of 2×10^4 cells/well in osteogenic medium. This medium was composed by growth medium supplemented with 5 μg ml^{-1} ascorbic acid (Gibco-Life Technologies) and 7 mM β-glycerophosphate (Sigma-Aldrich, Saint Louis, MO, USA). The cultures were kept at 37 °C in a humidified atmosphere of 5% CO_2 and 95% air, the medium was replaced every 48 h, and all assays were done on day 5.

2.2.2. Cell culture growth

Cell culture growth was assessed with a 3-[4,5-dimethylthiazol-2-yl]-2,5-diphenyl tetrazolium bromide (MTT, Sigma-Aldrich) assay. The MTT absorbance was measured as optical density at 570 nm using a μQuant plate reader (Biotek, Winooski, VT, USA). The data were collected in quintuplicate ($n = 5$).

2.2.3. In situ ALP activity

In situ ALP activity was analysed with a Fast Red assay. The cultures were washed in Hank's balanced salt solution (Sigma-Aldrich) and incubated for 30 min at 37 °C with 0.5 ml of 120 mM Tris buffer (Sigma-Aldrich), pH 8.4, containing 0.9 mM naphthol AS-MX phosphate (Sigma-Aldrich) and 1.8 mM Fast red TR (Sigma-Aldrich). The cells were washed and dried at room temperature. The images were obtained using a high-resolution camera (Canon EOS Digital Rebel,

Canon, Tokyo, Japan), processed and then quantified using Image J software [21]. The data were collected in quintuplicate ($n = 5$).

2.2.4. Gene expression of osteoblast markers

Gene expression of ALP, BSP, runt-related transcription factor 2 (RUNX2) and OPN was evaluated with real-time PCR. Total RNA (1 μg) was used to synthesize complementary DNA in a reverse transcription reaction (M–MLV reverse transcriptase, Promega Corporation, Madison, WI, USA). Real-time PCR was done using a CFX96 Real-Time PCR Detection System (Bio-Rad Laboratories, Philadelphia, PA, USA). Relative gene expression, which was collected in quadruplicate ($n = 4$), was normalized to the constitutive gene GAPDH, and the real change was relative to the gene expression of cells cultivated on Bioglass 45S5.

2.2.5. Detection of bone-related proteins

The proteins BSP and OPN were detected by immunofluorescence labelling. The cells were fixed, permeabilized and blocked with 5% non-fat powdered milk (Bio-Rad Laboratories). Then, the cells were incubated (1 h each incubation) with primary monoclonal antibodies anti-BSP (1:200, WVID1-9C5, Developmental Studies Hybridoma Bank—DSHB, Iowa City, IA, USA) and anti-OPN (1:200, MPIIIB10, DSHB). After that, cells were incubated with a mixture of the Alexa Fluor 594 (red fluorescence)-conjugated goat anti-mouse secondary antibody (1:200, Molecular Probes, Eugene, OR, USA) and Alexa Fluor 488 (green fluorescence)-conjugated phalloidin (1:200, Molecular Probes) to detect the actin cytoskeleton. Cell nuclei were stained with 300 nM 4′,6-diamidino-2-phenylindole, dihydrochloride (DAPI, Molecular Probes). The discs were observed using a fluorescence microscope Axio Imager M2 (Carl Zeiss), and the captured images were treated using Adobe Photoshop software.

The proteins ALP and RUNX2 were detected using Western blotting. A sample of total protein (70 μg) was submitted to electrophoresis in a denaturing 8.5% polyacrylamide gel. Then, proteins were transferred to a Hybond C-Extra membrane (GE Healthcare Life Science, Piscataway, NJ, USA) using a semidry transfer system (Bio-Rad Laboratories). ALP protein was detected after incubation of the membrane with mouse monoclonal anti-ALP antibody (1:2000, Santa Cruz Biotechnology, Santa Cruz, CA, USA), followed by a goat anti-mouse IgG HRP secondary antibody (1:2000, Santa Cruz Biotechnology). For RUNX2 detection, the incubation was made with rabbit monoclonal anti-RUNX2 (1:2500, Cell Signaling Technology, Danvers, MA, USA) followed by a goat anti-rabbit IgG secondary antibody (1:2500, Santa Cruz Biotechnology). Rabbit polyclonal anti-GAPDH (1:1000, Santa Cruz Biotechnology) followed by a goat anti-rabbit IgG HRP secondary antibody (1:3000, Santa Cruz Biotechnology) was used as a control. For detection of secondary antibodies, the western lightning chemiluminescence reagent (Perkin Elmer Life Sciences, Waltham, MA, USA) was used and the images were obtained using G-Box gel imaging (Syngene, Cambridge, United Kingdom). The quantification of ALP and RUNX2 expressions were performed by counting the number of pixels and normalized to GAPDH expression. The fold change was relative to the protein expression of cells cultivated on Bioglass 45S5.

2.2.6. Extracellular matrix mineralization

The Von Kossa staining was used to detect mineralized matrix. The cultures were incubated with silver nitrate (5 mg ml^{-1}) (Sigma-Aldrich), followed by hydroquinone (5 mg ml^{-1}) (Sigma-Aldrich) and sodium thiosulphate (50 mg ml^{-1}) (Sigma-Aldrich). After washing and drying at room temperature, the images were obtained using a camera (Canon EOS Digital Rebel), processed and quantified using Image J software [21]. The data were collected in quintuplicate ($n = 5$).

2.3. Osteoinductive potential of BioS-2P

2.3.1. Culture of MSCs

The Committee of Ethics in Animal Research of the School of Dentistry of Ribeirão Preto, University of São Paulo, Brazil, approved all of the experimental procedures performed with animals. Bone marrow MSCs harvested from the femur of two male Wistar rats weighing 150 g were cultivated in growth medium (non-osteogenic conditions) until subconfluence. MSCs of first passage were cultivated in 24-well culture plates on BioS-2P and Bioglass 45S5 discs and on polystyrene (control) at a cell density of 2×10^4 cells/well in growth medium. The cultures were kept at 37 °C in a humidified atmosphere of 5% CO_2 and 95% air. The medium was changed every 48 h, and all assays were done on day 10.

2.3.2. ALP activity

A commercial kit (Labtest Diagnostica SA, Lagoa Santa, MG, Brazil) was used to measure ALP activity by the release of thymolphthalein from thymolphthalein monophosphate. Absorbance was read at 590 nm using a μQuant plate reader (BioTek), and ALP activity was determined from a thymolphthalein standard curve. The data were collected in quintuplicate ($n = 5$) and are presented as ALP activity normalized to the total protein content, which was quantified in the same cell lysates using the Lowry method [22].

2.3.3. Gene expression of osteoblast markers

Gene expression of ALP, RUNX2, OPN and osteocalcin (OC) was evaluated in quadruplicate ($n = 4$) with real-time PCR, as described above (2.2.4). The cells cultured on polystyrene were used to calculate the real changes of gene expression.

2.4. Effects of BioS-2P scaffolds on bone repair

2.4.1. Surgical procedures for BioS-2P scaffold implantation

Fifteen male Wistar rats weighing 200–300 g were used for the following research protocols, which were approved by the Committee of Ethics in Research from the University of São Paulo. The animals were anesthetized with ketamine (7 mg/100 g body weight; Agener União, SP, Brazil) and xylazine (0.6 mg/100 g body weight; Calier, MG, Brazil). Calvarial bone defects that were 5 mm in diameter were unilaterally created with a trephine and implanted with BioS-2P scaffolds followed by a skin suture with nylon 4.0 (Ethicon Ltd, NJ, USA). Then, single doses of antibiotics and analgesics were administered. Four, 8 and 12 weeks post-implantation, the animals ($n = 5$ per period) were euthanized, and the samples were harvested and prepared for morphometric and histological analyses.

2.4.2. Morphometric and histological analyses

After harvesting, the samples were maintained in 10% formalin buffered with 0.1 M sodium cacodylate, pH 7.0. Morphometric analysis was performed with micro-CT using the SkyScan 1172 system (Bruker). The images and reconstructions were obtained as described above (2.1.2). Bone volume (BV), bone surface (BS), BS/BV ratio (BS/BV) BS/volume ratio (BV/VT), trabecular thickness (Tb.Th) and trabecular separation (Tb.Sp) of the newly formed bone were quantified using the 3D Ctan software 1.13.1.1.0 version (Bruker).

Histological analysis was carried out following a previously described protocol [23]. After micro-CT analysis, samples were kept in a solution of 70% ethanol for 72 h, followed by embedding in resin (LR White Hard Grade, London, UK) and sectioned using the Exakt Cutting System (Exakt, Norderstedt, Germany). The sections were polished, mounted on acrylic slides using the Exakt Grinding System (Exakt) and stained with Stevenel's blue and Alizarin red S. The tissues formed in the bone defects were histologically described using micrographs obtained with a Leica DMLB light microscope (Leica, Bensheim, Germany).

2.5. Effects of the association of BioS-2P with MSCs on bone repair

2.5.1. Cell incorporation in BioS-2P scaffolds

First-passage MSCs were obtained as described above (2.3.1), seeded by pipetting (2×10^5 cells/100 μl) into BioS-2P scaffolds, which were placed into 48-well and cultured for 18 h to allow cell adhesion. Cell incorporation was detected under epifluorescence using an ApoTome system and an Axiocam MRm digital camera (Zeiss). The efficiency of cell incorporation was evaluated by counting the non-incorporated cells that were enzymatically released from the 48-wells after BioS-2P scaffold removal. During the culture period, scaffolds were incubated at 37 °C in a humidified atmosphere of 5% CO_2 and 95% air for 24 h. BioS-2P scaffolds without cells were used as controls.

Table 1. Nominal compositions of BioS-2P and Bioglass 45S5.

Composition (mol %)	Na_2O	CaO	SiO_2	P_2O_5
BioS-2P	23.3	25.8	49.2	1.7
Bioglass 45S5	24.4	26.9	46.1	2.6

2.5.2. Cell tracking

MSCs were transduced using a lentiviral vector with luciferase 3–5 d after passage at a multiplicity of infection of 8. After 2 d, the medium was changed, and the cells were selected using puromycin during 6 d. These cells were seeded into BioS-2P scaffolds and surgically implanted into bone defects by following the same protocols described above (2.5.1 and 2.4.1, respectively). For cell tracking, luciferase-positive cells were detected from 6 h to 28 d after implantation using the IVIS imaging system (Xenogem Corporation, CA, USA) after 100 μl of a luciferin (mg ml^{-1}) local injection. Signal intensity was quantified as the photon flux (photons/s) within the region of interest by using IVIS Image 3.0 software (Caliper Life Sciences).

2.5.3. Surgical procedures for BioS-2P scaffolds with MSCs implantation

Five male Wistar rats weighing 200–300 g were used as described above (2.4.1). BioS-2P scaffolds seeded with unlabelled MSCs were implanted in rat calvarial defects, and 8 weeks post-implantation, the animals were euthanized, and the samples were collected and processed for histomorphometric and histological analyses. These data were compared to data from rats implanted with BioS-2P scaffolds without cells for 8 weeks.

2.6. Statistical analysis

Quantitative data were collected in quintuplicate ($n = 5$) for all parameters except gene expression, which were collected in quadruplicate ($n = 4$). The comparisons between two groups (BioS-2P versus Bioglass 45S5 and BioS-2P scaffold with MSCs versus BioS-2P without MSCs) were done using the Mann–Whitney test, whereas the Kruskal–Wallis test followed by the Student–Newman–Keuls test was used to compare three groups (BioS-2P, Bioglass 45S5 and polystyrene; 4, 8 and 12 weeks). The significance level was set at 5%.

3. Results

3.1. Characterization of BioS-2P

The nominal compositions of Na_2O, CaO, SiO_2 and P_2O_5 (mol %) of BioS-2P and Bioglass 45S5 are detailed in table 1. The XRD spectra showed that the

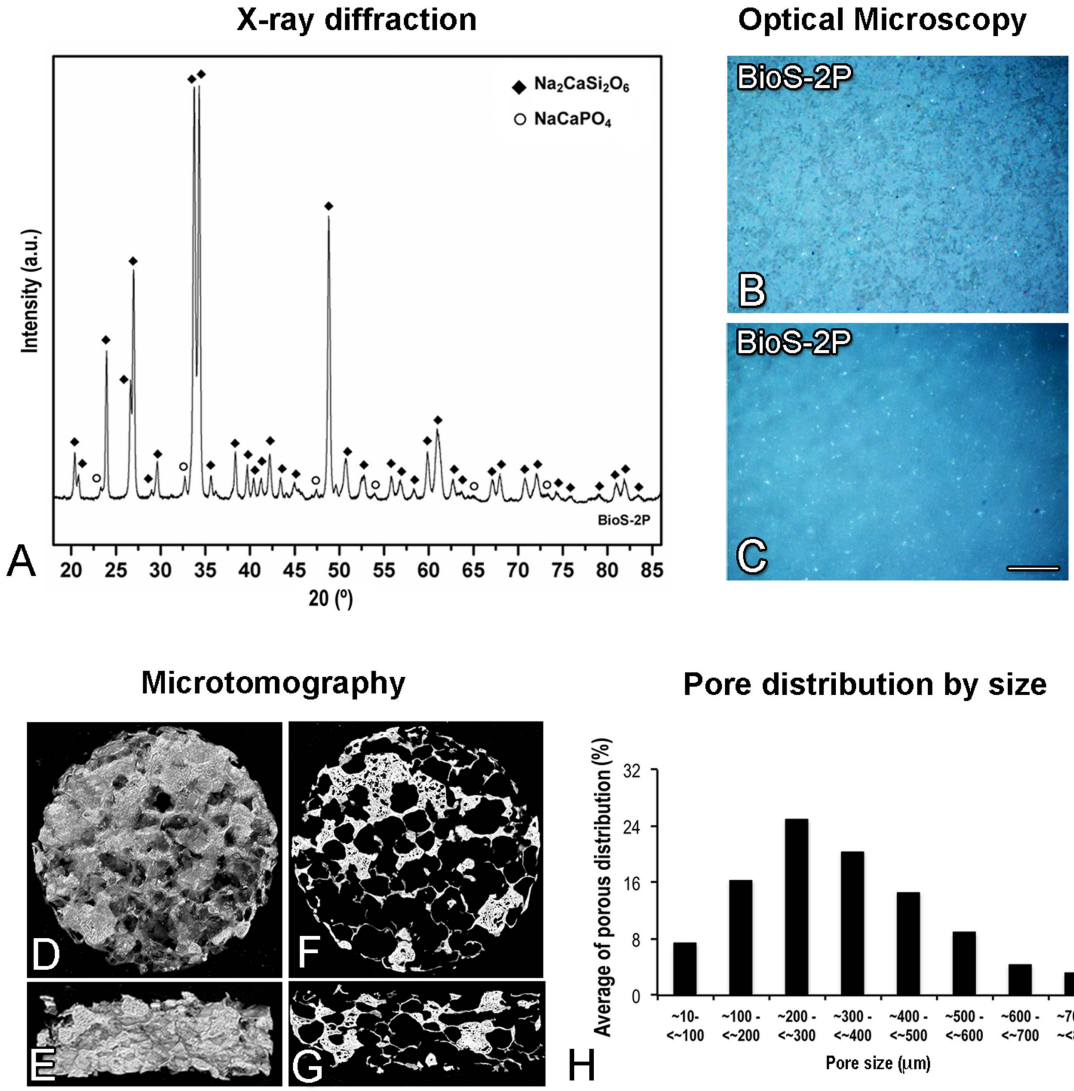

Figure 1. Characterization of the surfaces and scaffolds of Biosilicate® with two crystalline phases (BioS-2P). X-ray diffraction pattern of the BioS-2P surface (A). Optical microscopy of the surface of the BioS-2P disc (B) and a 3D-focused image obtained below the surface (C). Microtomography axial and sagittal images of the BioS-2P scaffold obtained from 3D reconstructions (D), (E) and 2D reconstructions (F), (G). Average pore distribution of BioS-2P scaffolds according to size (H). Scale bar B–C = 10 μm.

main crystalline phase in BioS-2P was a sodium calcium silicate ($Na_2CaSi_2O_6$–ICSD 060502) followed by a secondary crystalline phase ($NaCaPO_4$–ICSD 035629) that presented three main diffraction peaks at 23.3°, 32.7° and 47.5°, (figure 1(A)). The lower peak intensity of the secondary crystalline phase indicated that there was a lower crystallized volume fraction. Optical micrographs showed grains of $Na_2CaSi_2O_6$ at the surface of the BioS-2P (figure 1(B)) but no crystals of the secondary crystalline phase. However, at a submicron scale (approximately 0.2–0.4 μm) and below the surface, it was possible to observe the secondary crystalline phase due to its distinct optical behaviour. The bright spots that consisted of $NaCaPO_4$ were uniformly distributed in a matrix composed of $Na_2CaSi_2O_6$ crystals (figure 1(C)).

The micro-CT 3D and 2D images of the BioS-2P scaffolds showed a porous structure resembling a cancellous bone (figures 1(D)–(G)). The BioS-2P scaffold presented 76% ± 5% of porosity and pores with sizes ranging between 10 and 800 μm, whereas the majority of open pores were within 100 and 600 μm (figure 1(H)).

3.2. Osteogenic potential of BioS-2P

To determine osteogenic potential, UMR-106 osteoblastic cells were cultured on BioS-2P and Bioglass 45S5 discs under osteogenic conditions for 5 d. No difference in culture growth was detected between BioS-2P and Bioglass 45S5 ($p = 0.886$; figure 2(A)), whereas *in situ* ALP activity increased in cells cultured on BioS-2P compared to Bioglass 45S5 ($p = 0.029$; figure 2(B)). Higher gene expression for BSP ($p = 0.029$), RUNX2 ($p = 0.029$) and OPN ($p = 0.050$) was detected in cells cultured on BioS-2P compared to Bioglass 45S5, while no statistically significant difference in the expression of ALP was

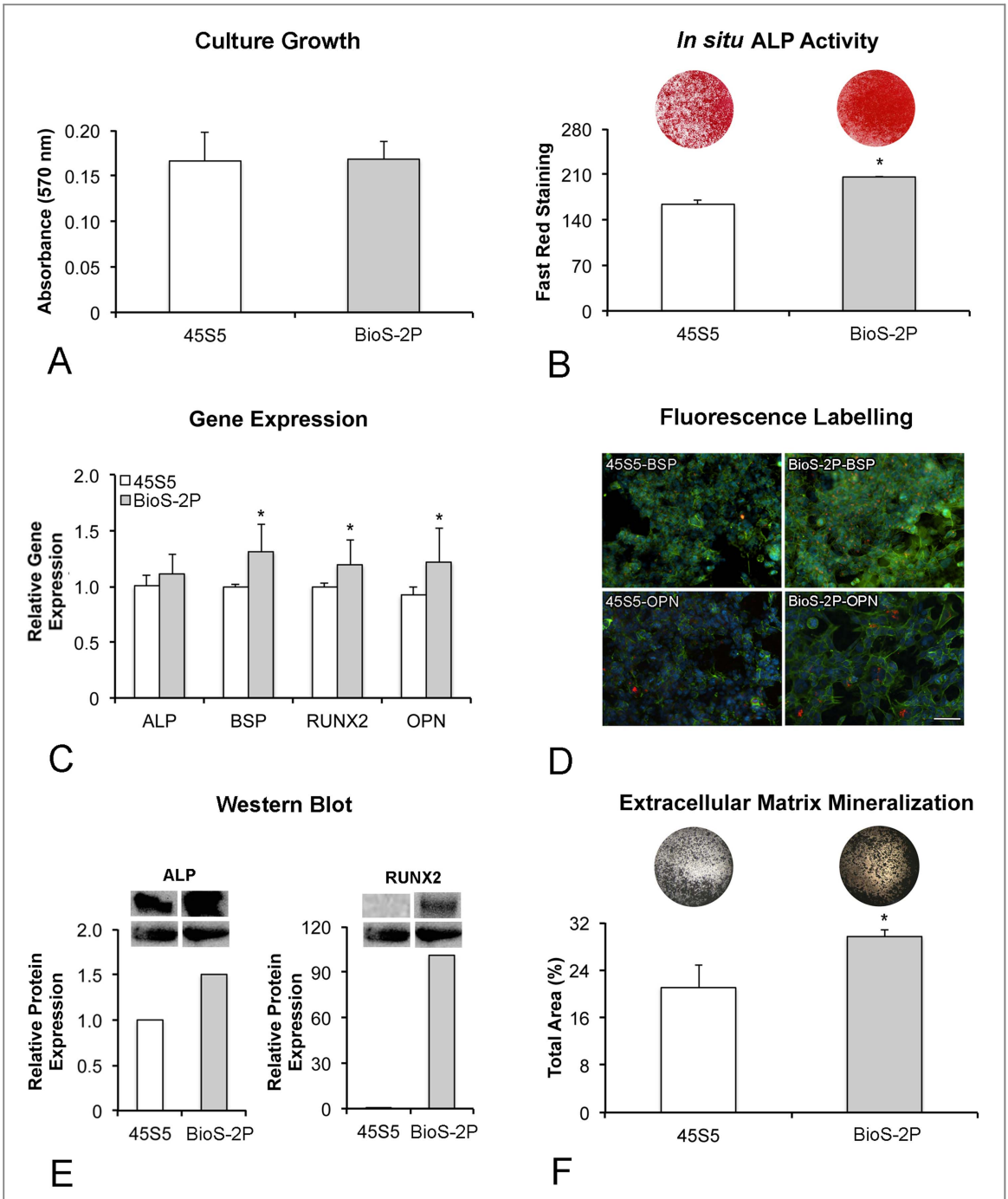

Figure 2. Osteogenic potential of Biosilicate® with two crystalline phases (BioS-2P). Culture growth (A), *in situ* alkaline phosphatase (ALP) activity (B), gene expression of ALP, bone sialoprotein (BSP), runt-related transcription factor 2 (RUNX2) and osteopontin (OPN) (C), BSP and OPN protein detection (D), ALP and RUNX2 protein detection (E), and extracellular matrix mineralization (F) of UMR-106 osteoblastic cells cultured on Bioglass 45S5 and BioS-2P on day 5. The data are showed as the mean ± standard deviation (A)–(C) and (F), and statistically significant differences are indicated by asterisks ($p \leqslant 0.05$). *D*: red fluorescence—BSP or OPN protein, as indicated; green fluorescence—actin cytoskeleton; blue fluorescence—nucleus. Scale bar $D = 50$ μm.

observed between the bioactive surfaces ($p = 0.200$) (figure 2(C)). BSP and OPN proteins were detected in cells cultivated on both surfaces with marked expression on BioS-2P compared to Bioglass 45S5 (figure 2(D)). Higher protein expression of ALP and RUNX2 was also observed in cells cultured on BioS-2P compared to Bioglass 45S5 (figure 2(E)). Extracellular matrix mineralization increased in cells cultured on BioS-2P compared to Bioglass 45S5 ($p = 0.029$; figure 2(F)).

3.3. Osteoinductive potential of BioS-2P

To determine osteoinductive potential, MSCs were cultured on BioS-2P, Bioglass 45S5 and polystyrene under non-osteogenic conditions for 10 d. The ALP activity was greater in cells cultured on Bioglass 45S5 compared to BioS-2P and lower in cells cultured on polystyrene ($p = 0.001$; figure 3(A)). Furthermore, the gene expression of all evaluated osteoblast markers was higher on bioactive glasses than on polystyrene ($p = 0.001$ for all genes; figures 3(B)–(E)). By comparing

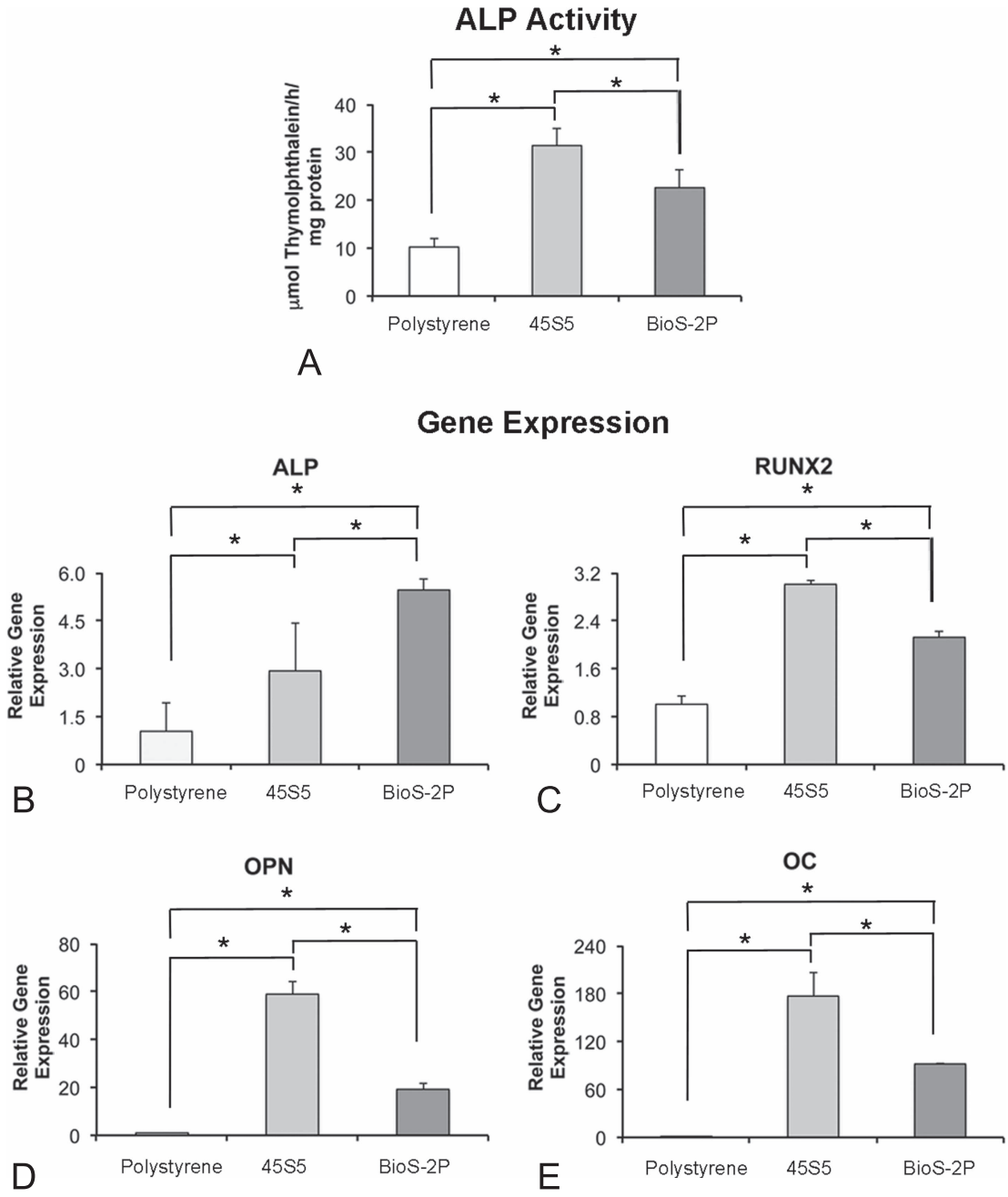

Figure 3. Osteoinductive potential of Biosilicate® with two crystalline phases (BioS-2P). Alkaline phosphatase (ALP) activity (A) and gene expression of ALP (B), runt-related transcription factor 2 (RUNX2) (C), osteopontin (OPN) (D) and osteocalcin (OC) (E) of mesenchymal stem cells (MSCs) cultured on polystyrene, Bioglass 45S5 and BioS-2P on day 10. The data are showed as the mean ± standard deviation, and statistically significant differences are indicated by asterisks ($p \leqslant 0.05$).

only the bioactive materials, the gene expression of ALP was higher in cells cultured on BioS-2P, whereas RUNX2, OPN and OC expression was higher on Bioglass 45S5 (figure 3(B)).

3.4. Effects of the BioS-2P scaffold on bone repair

Three-dimensional micro-CT images demonstrated that BioS-2P promoted bone repair (figures 4(A)–(C)). Morphometric analysis showed there were no differences in all evaluated parameters, irrespective of time (BS $p = 0.733$; BV $p = 0.121$; BS/BV $p = 0.208$; BV/TV $p = 0.904$; Tb.Th $p = 0.274$; Tb.Sp $p = 0.482$) (figures 4(D)–(I)). The histological observations confirmed the micro-CT findings, and although the axial images showed bone formation in the centre of the bone defect (figures 5(A)–(C)), the transversal slices revealed that BioS-2P scaffolds remarkably improved bone formation that was integrated with the parent lamellar bone at the defect margins (figures 5(D)–(F)). Higher magnifications showed cancellous bone in direct contact with BioS-2P (figures 5(G)–(I)).

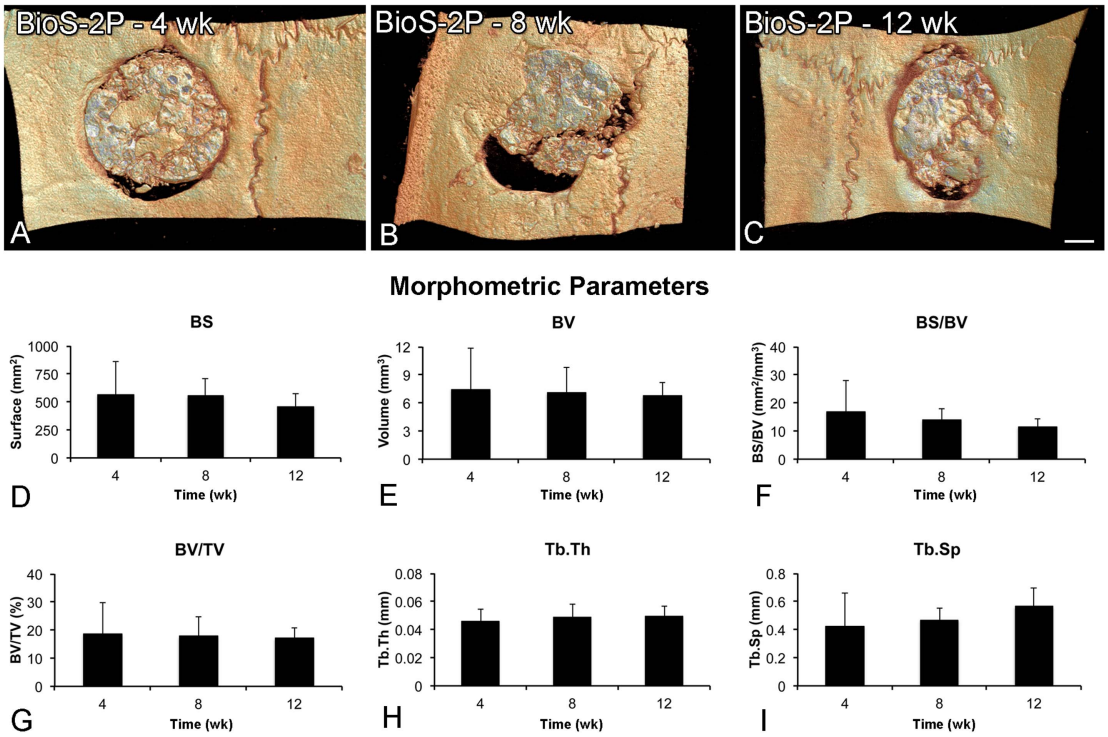

Figure 4. 3D-reconstructed microtomography images of rat calvarial bone defects implanted with BioS-2P after 4 (A), 8 (B) and 12 (C) weeks were used to evaluate the bone surface (BS) (D), bone volume (BV) (E), bone surface/bone volume (BS/BV) (F), bone surface/tissue volume (BS/TV) (G), trabecular thickness (Tb.Th) (H) and trabecular separation (Tb.Sp) (I). The data are showed as the mean ± standard deviation, and there were no statistically significant differences for any evaluated parameter ($p \leqslant 0.05$). Scale bar A–C = 1 mm.

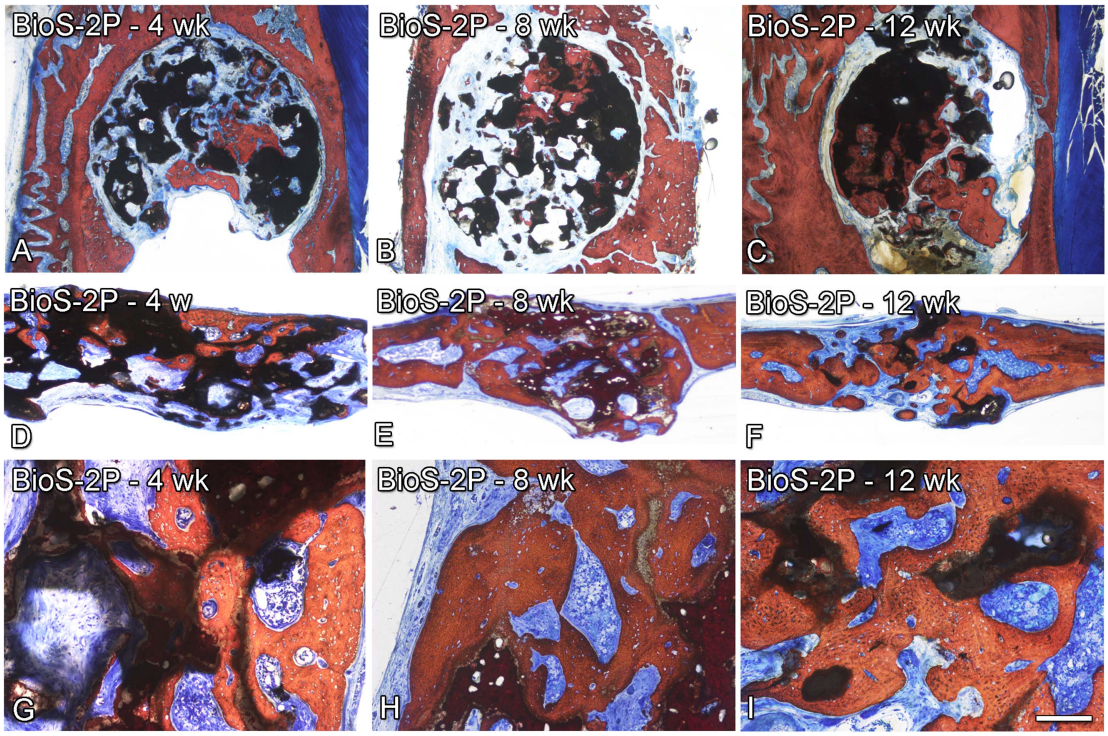

Figure 5. Light microscopy images of rat calvarial bone defects implanted with BioS-2P after 4 (A), (D), (G), 8 (B), (E), (H) and 12 (C), (F), (I) weeks. Asterisks indicate the newly formed bone and arrows indicate this new bone in close contact with the material surface. Scale bar = 100 μm.

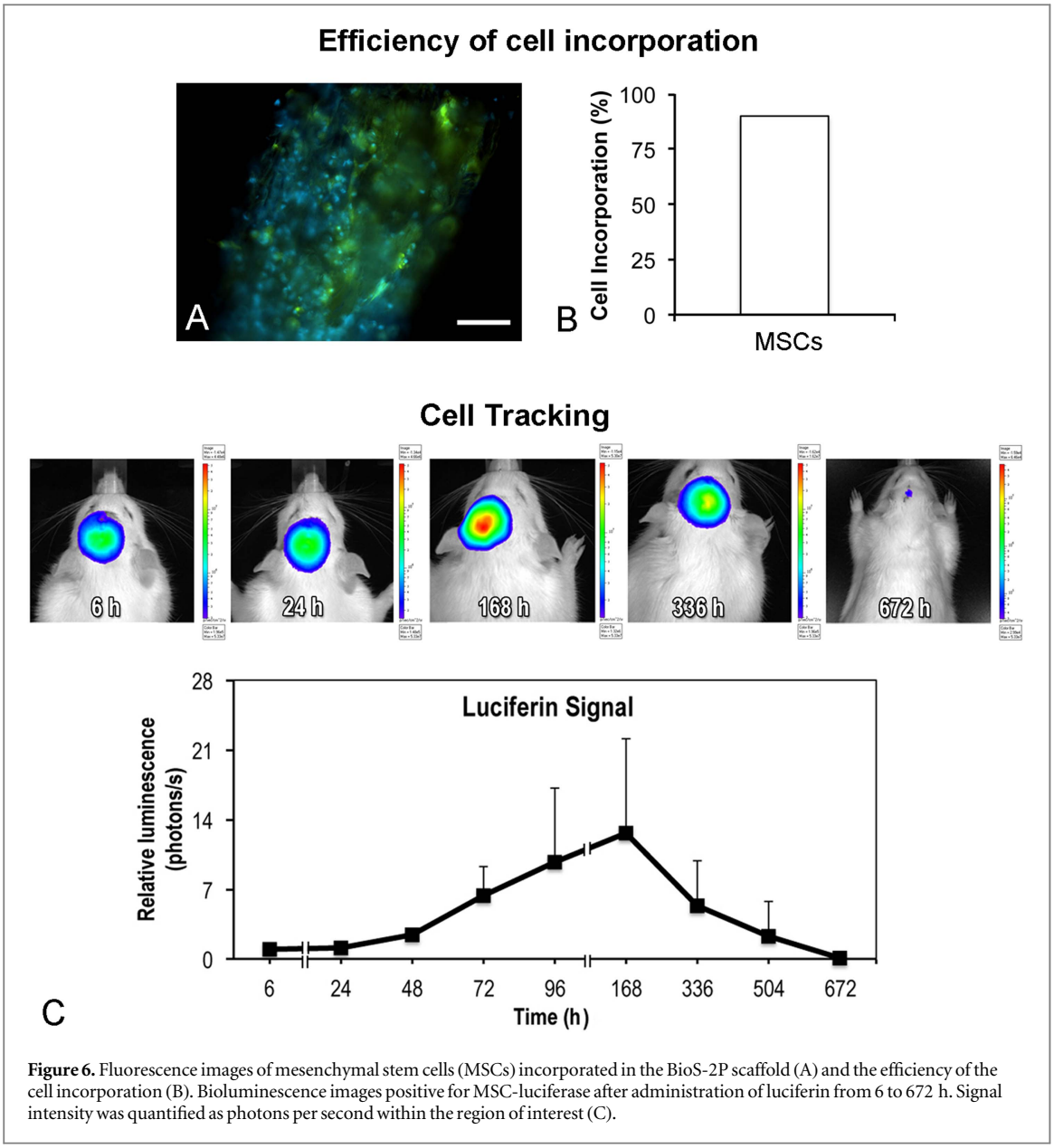

Figure 6. Fluorescence images of mesenchymal stem cells (MSCs) incorporated in the BioS-2P scaffold (A) and the efficiency of the cell incorporation (B). Bioluminescence images positive for MSC-luciferase after administration of luciferin from 6 to 672 h. Signal intensity was quantified as photons per second within the region of interest (C).

3.5. Effects of the association of BioS-2P scaffold and MSCs on bone repair

MSCs could be seen within the pores of BioS-2P scaffolds (figure 6(A)), and around of 80% of the seeded cells were incorporated into the scaffolds (figure 6(B)). Cell tracking showed that MSCs were detected in the bone defects for 4 weeks with a peak at 1 week (figure 6(C)). Reconstructed images generated by micro-CT showed that the BioS-2P scaffold alone or combined with MSCs promoted similar bone repair (figures 7(A)–(B)). Morphometric analysis confirmed this observation because no differences in all evaluated parameters were found despite the presence of cells (BS $p = 0.589$; BV $p = 0.180$; BS/BV $p = 0.589$; BV/TV = 0.180; Tb.Th $p = 0.818$; Tb.Sp $p = 0.937$) (figures 7(C)–(H)). The histological observations confirmed the micro-CT findings. The axial images showed bone formation in the centre and at the border of the bone defects (figures 8(A)–(B)). Higher magnifications showed a direct contact between bone tissue and BioS-2P (figures 8(C)–(D)).

4. Discussion

Here, we reported that BioS-2P had a secondary crystalline phase and presented an architecture that resembled a cancellous bone. BioS-2P displayed *in vitro* osteogenic and osteoinductive properties and enhanced the repair of bone tissue in a rat calvarial defect model. Under standard osteogenic conditions, BioS-2P stimulated the osteoblast activity of the UMR-106 cell line and generated a microenvironment that promoted the induction of osteoblast phenotype and genotype expression in MSCs grown without osteogenic factors. We also noticed that the BioS-2P scaffold is able to stimulate bone formation in such magnitude that its association with MSCs was not able to increase.

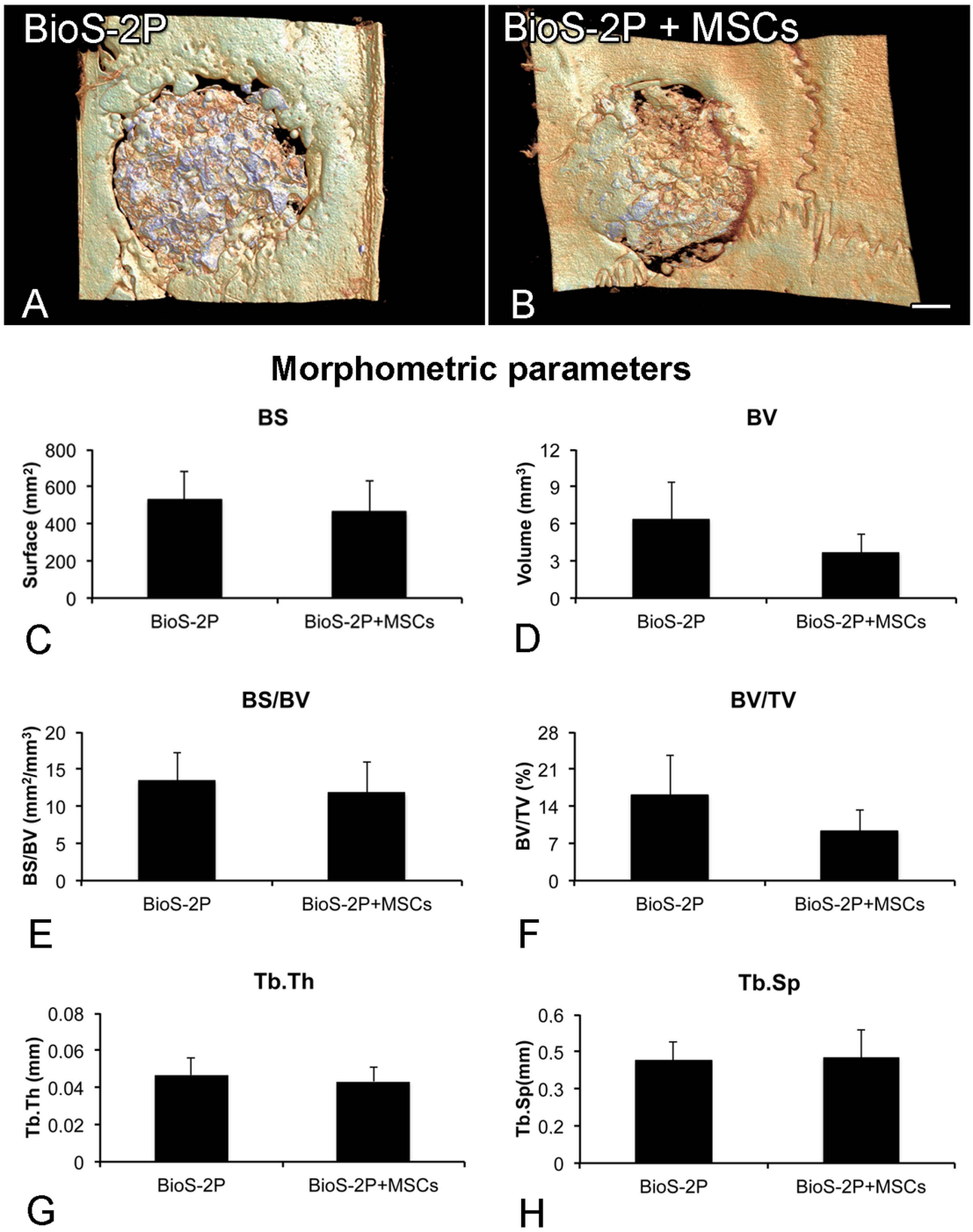

Figure 7. 3D-reconstructed microtomography images of rat calvarial bone defects implanted with BioS-2P (A) or BioS-2P associated with mesenchymal stem cells (MSCs, B) after 8 weeks. These images were used to evaluate bone surface (BS) (C), bone volume (BV) (D), bone surface/bone volume (BV/BV) (E), bone surface/tissue volume (BS/TV) (F), trabecular thickness (Tb.Th) (G) and trabecular separation (Tb.Sp) (H). The data are showed as the mean ± standard deviation, and there were no statistically significant differences in any evaluated parameters ($p \leqslant 0.05$). Scale bar A–B = 1 mm.

We confirmed that the secondary crystalline phase present in BioS-2P was a sodium-calcium phosphate ($NaCaPO_4$) that was difficult to identify due to its low crystallized volume fraction. This phase was also detected in Bioglass 45S5 as well as in other glass-ceramics after heat treatment at temperatures of approximately 1000 °C, and the phase was identified as α- or β-rhenanite [24–27]. The secondary crystalline phase was highly reactive in simulated body fluid and acted as a heterogeneous nuclei for hydroxycarbonate apatite growth at glass-ceramic surfaces, including Biosilicate® [16, 27, 28], and it improved the mechanical strength, elastic modulus and fracture toughness without affecting the bioactivity index [14]. These features favoured scaffold fabrication with ideal porosity and a porous network, which were able to maintain their integrity [29], while cell activities such as migration, grown and differentiation occurred [29–31].

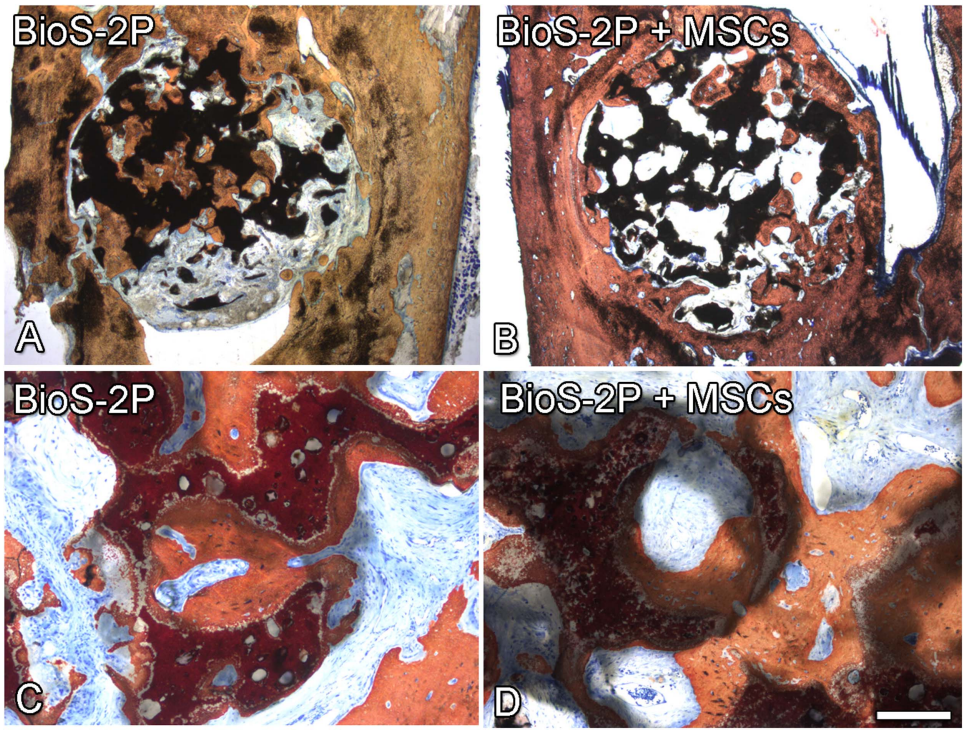

Figure 8. Light microscopy images of rat calvarial bone defects implanted with BioS-2P and BioS-2P associated with mesenchymal stem cells (B) for 8 weeks. Asterisks indicate the newly formed bone and arrows indicate this new bone in close contact with the material surface. Scale bar = 100 μm.

The ability of scaffolds to be populated by osteoblasts is very important for therapies that aim to regenerate bone tissue. Our results showed a similar pattern of culture growth on BioS-2P and on Bioglass 45S5 discs. In a previous study, it was observed that osteoblasts derived from rat calvarial cells grown on BioS-1P and Bioglass 45S5 exhibited the same proliferation rate [17]. These findings strongly suggested that the presence of one or two crystalline phases did not impact the capacity of Biosilicate® to support cell attachment and proliferation. In both situations, the dynamics of growth followed the growth for Bioglass 45S5.

Bioactive glasses can induce osteoblast differentiation and extracellular matrix mineralization [17, 32]. To track the role of BioS-2P in driving osteoblast functions in UMR-106 cells, we analysed the activity of ALP, which is a key enzyme in the process of mineralization [33]. Higher ALP activity was detected in BioS-2P, which could lead to a higher extracellular matrix mineralization because of a direct positive correlation between these two parameters in different experimental designs [34, 35]. Additionally, the release of ionic dissolution products by bioactive glasses and glass-ceramics may affect the gene expression profile of osteogenic cells [36–39]. Thus, to further investigate the osteoblast phenotype and genotype regulation induced by BioS-2P, we examined the gene and protein expressions of ALP, BSP, RUNX2 and OPN, which are key markers expressed during the time course of osteoblast differentiation. In general, our results showed that BioS-2P increased the gene and protein expressions of all evaluated markers compared to Bioglass 45S5, which suggested that BioS-2P presented higher osteogenic potential than Bioglass 45S5.

Among different bioactive glass compositions, the glass-ceramic in the Na_2O–CaO–SiO_2–P_2O_5 system mimicked the microenvironment created by the osteogenic medium and may consequently dictate the fate of MSCs [32]. Based on this possibility and on the osteogenic potential of BioS-2P, we cultured MSCs in non-osteogenic medium to investigate the hypothesis that BioS-2P by itself could affect osteoblast differentiation. In addition to using polystyrene as a control, BioS-2P was also compared to Bioglass 45S5 to determine the osteoinductive potential of both materials. We observed that BioS-2P upregulated ALP activity and the gene expression of ALP, RUNX2, OPN and OC compared to polystyrene. Although the ALP activity and the expression of the majority of genes were higher for Bioglass 45S5 compared to BioS-2P, our results clearly showed the ability of BioS-2P to induce osteoblast differentiation in MSCs. Similar to these results, another study showed that Bioglass 45S5-conditioned medium favours osteoblast differentiation in the absence of osteogenic factors [40].

Beyond the *in vitro* osteogenic and osteoinductive properties, the BioS-2P scaffold promoted *in vivo* bone formation. It was noteworthy that many areas of bone formation were seen at the centre of the defects and were not related to the parent bone, which

suggested BioS-2P had a stimulatory effect. Additionally, the observation of direct contact between the BioS-2P surface and bone corroborated the beneficial effects of BioS-2P. However, the effects of BioS-2P were somewhat limited, so no fully defective regeneration was observed, and there was no increase in bone formation during the implantation time. Similar to this outcome, meaningful bone formation was observed for BioS-1P and BioS-2P implanted in rabbit femurs and rat tibias [19, 41].

The effects of combining scaffolds and cells on bone formation have produced contradictory outcomes. Some studies reported synergistic effects [42–46], while others failed to show improved bone formation when MSCs were combined with scaffolds [31, 47, 48]. Our results aligned with the latter studies because the combination of BioS-2P with MSCs did not increase bone repair. This result could have arisen, at least in part, due to the absence of cells, the scaffold architecture or the number of seeded cells [47]. However, it is most likely that none of these factors played a role in this study. The BioS-2P scaffold presented physical characteristics close to the ideal in terms of porosity and pore size. The incorporation method allowed for seeding approximately 80% of the cells to the scaffolds, and the cell tracking showed that the cells were present in the defects for a long time. It seems that the stimulatory effect of the BioS-2P on bone healing could not be enhanced by the addition of MSCs due to modifications in the microenvironment caused by the dissolution products of glassy materials that may have masked the cellular effects [39, 49]. On the other hand, it is not possible to rule out that by using a higher cell density, a synergistic effect could be detected.

5. Conclusion

We showed that BioS-2P displayed a sodium-calcium silicate and a sodium-calcium phosphate phase, and BioS-2P could be used to manufacture three-dimensional scaffolds with an architecture resembling cancellous bone. BioS-2P permitted culture growth and stimulated osteoblast activity under osteogenic conditions, while generating an osteoinductive microenvironment that drove MSC differentiation into osteoblasts under non-osteogenic conditions. BioS-2P was able to stimulate meaningful formation of bone tissue in rat calvarial defects despite the presence of cells. Considering the suitability of this new biomaterial for use in the design of scaffolds, these findings open windows for evaluating the effectiveness of BioS-2P in bone regeneration based on tissue engineering concepts.

Acknowledgments

This study was supported by the São Paulo Research Foundation (Grants # 2012/23879-5 and 2012/23525-9, 2013/07793-6, FAPESP, Brazil). The authors thank Rafael Peixoto dos Santos for his assistance in the preparation of the glass and glass-ceramic discs as well as Fabiola Singaretti de Oliveira and Roger Rodrigo Fernandes for their technical assistance in the biological experiments.

Conflicts of interest

No conflicts of interest are declared.

References

[1] Langer R and Vacanti J P 1993 Tissue engineering *Science* **260** 920–6
[2] Hollister S J *et al* 2005 Engineering craniofacial scaffolds *Orthod. Craniofac. Res.* **8** 162–73
[3] Bose S, Roy M and Bandyopadhyay A 2012 Recent advances in bone engineering scaffolds *Trends Biotechnol.* **30** 546–54
[4] Tevlin R, McArdle A, Atashroo D, Walmsley G G, Senarath-Yapa K, Zielins E R, Paik K J, Longaker M T and Wan D C 2014 Biomaterials for craniofacial bone engineering *J. Dent. Res.* **93** 1187–95
[5] Hench L L 2013 Chronology of bioactive glass development and clinical applications *New. J. Glass. Ceram.* **3** 67–73
[6] Baino F, Novajra G, Miguez-Pacheco V, Boccaccini A R and Vitale-Brovarone C 2016 Bioactive glasses: special applications outside the skeletal system *J. Non-Cryst. Solids* **15** 15–30
[7] Hench L L, Splinter R J, Allen W C and Greenlee T K 1971 Bonding mechanisms at the interface of ceramic prosthetic materials *J. Biomed. Mater.* **5** 117–41
[8] Hench L L and Jones J R 2015 Bioactive glasses: frontiers and challenges *Front. Bioeng. Biotechnol.* **3** 194
[9] Reilly G C, Radin S, Chen A T and Ducheyne P 2007 Differential alkaline phosphatase responses of rat and human bone marrow derived mesenchymal stem cells to 45S5 bioactive glass *Biomaterials* **28** 4091–7
[10] Chen Q Z, Thompson I D and Boccaccini A R 2006 45S5 Bioglass®-derived glass-ceramic scaffolds for bone tissue engineering *Biomaterials* **27** 2414–25
[11] Baino F and Vitale-Brovarone C 2011 Three-dimensional glass-derived scaffolds for bone tissue engineering: current trends and forecasts for the future *J. Biomed. Mater. Res.* A **97** 514–35
[12] Hum J and Boccaccini A R 2012 Bioactive glasses as carriers for bioactive molecules and therapeutic drugs: a review *J. Mater. Sci., Mater. Med.* **23** 2317–33
[13] Nganga S, Zhang D, Moritz N, Vallittu P K and Hupa L 2012 Multi-layer porous fiber-reinforced composites for implants: *in vitro* calcium phosphate formation in the presence of bioactive glass *Dent. Mater.* **28** 1134–45
[14] Peitl-Filho O, Zanotto E D and Hench L L 1997 Bioactive ceramics and method for preparing bioactive ceramics *US Patent* WO 97/41079
[15] Peitl-Filho O, Zanotto E D and Hench L L 2001 Highly bioactive P_2O_5–Na_2O–CaO–SiO_2 glass-ceramics *J. Non-Cryst. Solids* **292** 115–26
[16] Crovace M C, Sousa M T, Chinaglia C R, Peitl O and Zanotto E D 2016 Biosilicate®—a multipurpose, highly bioactive glass-ceramic. *In vitro*, *in vivo* and clinical trials *J. Non-Cryst. Solids* **432** 90–110
[17] Moura J, Teixeira L N, Ravagnani C, Peitl O, Zanotto E D, Beloti M M, Panzeri H, Rosa A L and de Oliveira P T 2007 *In vitro* osteogenesis on a highly bioactive glass-ceramic (Biosilicate) *J. Biomed. Mater. Res.* A **82** 545–57
[18] Roriz V M, Rosa A L, Peitl O, Zanotto E D, Panzeri H and de Oliveira P T 2010 Efficacy of a bioactive glass-ceramic (Biosilicate) in the maintenance of alveolar ridges and in osseointegration of titanium implants *Clin. Oral Implants Res.* **21** 148–55

[19] Azenha M R, Peitl O and Barros V M 2010 Bone response to biosilicates with different crystal phases *Braz. Dent. J.* **21** 383–9
[20] Kido H W *et al* 2015 Porous bioactive scaffolds: characterization and biological performance in a model of tibial bone defect in rats *J. Mater. Sci., Mater. Med.* **26** 74
[21] Schneider C A, Rasband W S and Eliceiri K W 2012 NIH image to ImageJ: 25 years of image analysis *Nat. Methods* **9** 671–5
[22] Lowry O H, Rosebrough N J, Farr A L and Randall R J 1951 Protein measurement with the folin phenol reagent *J. Biol. Chem.* **193** 265–75
[23] Maniatopoulos C, Rodriguez A, Deporter D A and Melcher A H 1986 An improved method for preparing histological sections of metallic implants *Int. J. Oral Maxillofac. Implants* **1** 31–7
[24] O'Donnell M D, Watts S J, Law R V and Hill R G 2008 Effect of P_2O_5 content in two series of soda lime phosphosilicate glasses on structure and properties: II. Physical properties *J. Non-Cryst. Solid* **354** 3561–6
[25] Ho W, Rheinberger V, Wegner S and Frank M 2000 Needle-like apatite-leucite glass-ceramic as a base material for the veneering of metal restorations in dentistry *J. Mater. Sci. Mater. Med.* **11** 11–7
[26] Höland W, Rheinberger V and Frank M 1999 Mechanisms of nucleation and controlled crystallization of needle-like apatite in glass-ceramics of the SiO_2–Al_2O_3–K_2O–CaO–P_2O_5 system *J. Non-Cryst. Solid* **253** 170–7
[27] Höland W, Rheinberger V, Apel E, Hoen C, Höland M, Dommann A, Obrecht M, Mauth C and Graf-Hausner U 2006 Clinical applications of glass-ceramics in dentistry *J. Mater. Sci., Mater. Med.* **17** 1037–42
[28] Höland M, Dommann A, Höland W, Apel E and Rheinberger V 2005 Microstructure formation and surface properties of a rhenanite-type glass-ceramic containing 6.0 wt% P_2O_5 *Glass Sci. Technol.* **78** 153–8
[29] Rezwan K, Chen Q Z, Blaker J J and Boccaccini A R 2006 Biodegradable and bioactive porous polymer/inorganic composite scaffolds for bone tissue engineering *Biomaterials* **27** 3413–31
[30] Karageorgiou V and Kaplan D 2005 Porosity of 3D biomaterial scaffolds and osteogenesis *Biomaterials* **26** 5474–91
[31] Kasten P, Beyen I, Niemeyer P, Luginbühl R, Bohner M and Richter W 2008 Porosity and pore size of beta-tricalcium phosphate scaffold can influence protein production and osteogenic differentiation of human mesenchymal stem cells: an *in vitro* and *in vivo* study *Acta Biomater.* **4** 1904–15
[32] Meseguer-Olmo L, Bernabeu-Esclapez A, Ros-Martinez E, Sánchez-Salcedo S, Padilla S, Martín A I, Vallet-Regí M, Clavel-Sainz M, Lopez-Prats F and Meseguer-Ortiz C L 2008 *In vitro* behaviour of adult mesenchymal stem cells seeded on a bioactive glass-ceramic in the SiO_2-CaO-P_2O_5 system *Acta Biomater.* **4** 1104–13
[33] Beck G R Jr, Sullivan E C, Moran E and Zerler B 1998 Relationship between alkaline phosphatase levels, osteopontin expression, and mineralization in differentiating MC3T3-E1 osteoblasts *J. Cell. Biochem.* **68** 269–80
[34] Boyan B D, Bonewald L F, Paschalis E P, Lohmann C H, Rosser J, Cochran D L, Dean D D, Schwartz Z and Boskey A L 2002 Osteoblast-mediated mineral deposition in culture is dependent on surface microtopography *Calcif. Tissue Int.* **71** 519–29
[35] Zhang J, Doll B A, Beckman E J and Hollinger J O 2003 A biodegradable polyurethane-ascorbic acid scaffold for bone tissue engineering *J. Biomed. Mater. Res.* A **67** 389–400
[36] Xynos I D, Hukkanen M V, Batten J J, Buttery L D, Hench L L and Polak J M 2000 Bioglass 45S5 stimulates osteoblast turnover and enhances bone formation: *in vitro* implications and applications for bone tissue engineering *Calcif. Tissue Int.* **64** 321–29
[37] Xynos I D, Edgar A J, Buttery L D, Hench L L and Polak J M 2001 Gene-expression profiling of human osteoblasts following treatment with the ionic products of Bioglass 45S5 dissolution *J. Biomed. Mater. Res.* **55** 151–7
[38] Hench L L, Xynos I D and Polak J M 2004 Bioactive glasses for *in situ* tissue regeneration *J. Biomater. Sci. Polym. Ed.* **15** 543–62
[39] Hoppe A, Güldal N S and BoccaccinI A R 2011 A review of the biological response to ionic dissolution products from bioactive glasses and glass-ceramics *Biomaterials* **32** 2757–74
[40] Tsigkou O, Jones J R, Polak J M and Stevens M M 2009 Differentiation of fetal osteoblasts and formation of mineralized bone nodules by 45S5 Bioglass conditioned medium in the absence of osteogenic supplements *Biomaterials* **30** 3542–50
[41] Granito R N *et al* 2011 *In vivo* biological performance of a novel highly bioactive glass-ceramic (Biosilicate): a biomechanical and histomorphometric study in rat tibial defects *J. Biomed. Mater. Res.* B **97** 139–47
[42] Beloti M M, Sicchieri L G, de Oliveira P T and Rosa A L 2012 The influence of osteoblast differentiation stage on bone formation in autogenously implanted cell-based poly(lactide-co-glycolide) and calcium phosphate constructs *Tissue Eng.* A **18** 999–1005
[43] El-Gendy R, Yang X B, Newby P J, Boccaccini A R and Kirkham J 2013 Osteogenic differentiation of human dental pulp stromal cells on 45S5 Bioglass® based scaffolds *in vitro* and *in vivo Tissue Eng.* A **19** 707–15
[44] Eldesoqi K, Henrich D, El-Kady A M, Arbid M S, Abd El-Hady B M, Marzi I and Seebach C 2014 Safety evaluation of a bioglass-polylactic acid composite scaffold seeded with progenitor cells in a rat skull critical-size bone defect *PLoS One* **9** e87642
[45] García-Gareta E, Coathup M J and Blunn G W 2015 Osteoinduction of bone grafting materials for bone repair and regeneration *Bone* **81** 112–21
[46] Santos T S, Abuna R P F, Lopes H B, Almeida A L G, Beloti M M and Rosa A L 2015 Association of mesenchymal stem cells and osteoblasts for bone repair *Regen. Med.* **10** 127–33
[47] Rathbone C R, Guda T, Singleton B M, Oh D S, Appleford M R, Ong J L and Wenke J C 2014 Effect of cell-seeded hydroxyapatite scaffolds on rabbit radius bone regeneration *J. Biomed. Mater. Res.* A **102** 1458–66
[48] Rai B, Lin J L, Lim Z X, Guldberg R E, Hutmacher D W and Cool S M 2010 Differences between *in vitro* viability and differentiation and *in vivo* bone-forming efficacy of human mesenchymal stem cells cultured on PCL-TCP scaffolds *Biomaterials* **31** 7960–70
[49] Todeschi M R, El Backly R, Capelli C, Daga A, Patrone E, Introna M, Cancedda R and Mastrogiacomo M 2015 Transplanted umbilical cord mesenchymal stem cells modify the *in vivo* microenvironment enhancing angiogenesis and leading to bone regeneration *Stem Cells Dev.* **24** 1570–81